



THE UNIVERSITY *of* EDINBURGH

Edinburgh Research Explorer

Luminosity function and radial distribution of Milky Way satellites in a CDM Universe

Citation for published version:

Maccio', AV, Kang, X, Fontanot, F, Somerville, RS, Koposov, SE & Monaco, P 2010, 'Luminosity function and radial distribution of Milky Way satellites in a CDM Universe', *Monthly Notices of the Royal Astronomical Society*. <https://doi.org/10.1111/j.1365-2966.2009.16031.x>

Digital Object Identifier (DOI):

[10.1111/j.1365-2966.2009.16031.x](https://doi.org/10.1111/j.1365-2966.2009.16031.x)

Link:

[Link to publication record in Edinburgh Research Explorer](#)

Document Version:

Peer reviewed version

Published In:

Monthly Notices of the Royal Astronomical Society

General rights

Copyright for the publications made accessible via the Edinburgh Research Explorer is retained by the author(s) and / or other copyright owners and it is a condition of accessing these publications that users recognise and abide by the legal requirements associated with these rights.

Take down policy

The University of Edinburgh has made every reasonable effort to ensure that Edinburgh Research Explorer content complies with UK legislation. If you believe that the public display of this file breaches copyright please contact openaccess@ed.ac.uk providing details, and we will remove access to the work immediately and investigate your claim.



Luminosity function and radial distribution of Milky Way Satellites in a Λ CDM Universe

Andrea V. Macciò^{1*}, Xi Kang¹, Fabio Fontanot¹, Rachel S. Somerville^{1,2}
Sergey Koposov^{1,3,4}, Pierluigi Monaco^{5,6}

¹ *Max-Planck-Institut für Astronomie, Königstuhl 17, 69117 Heidelberg, Germany*

² *Space Telescope Science Institute, 3700 San Martin Drive, Baltimore, MD 21218, USA*

³ *Institute of Astronomy, University of Cambridge, Madingley Road, Cambridge, UK*

⁴ *Sternberg Astronomical Institute, Universitetskij pr. 13, 119992 Moscow, Russia*

⁵ *Dipartimento di Astronomia, Università di Trieste, via Tiepolo 11, 34131 Trieste, Italy*

⁶ *INAF-Osservatorio Astronomico, Via Tiepolo 11, I-34131 Trieste, Italy*

submitted to MNRAS

ABSTRACT

We study the luminosity function and the radial distribution of satellite galaxies within Milky Way sized haloes as predicted in Cold Dark Matter based models of galaxy formation, making use of numerical N-body techniques as well as three different semi-analytic model (SAMs) galaxy formation codes. We extract merger trees from very high-resolution dissipationless simulations of four Galaxy-sized DM haloes, and use these as common input for the semi-analytic models. We present a detailed comparison of our predictions with the observational data recently obtained on the Milky Way satellite luminosity function (LF). We find that semi-analytic models with rather standard astrophysical ingredients are able to reproduce the observed luminosity function over six orders of magnitude in luminosity, down to magnitudes as faint as $M_V = -2$. We also perform a comparison with the actual observed number of satellites as a function of luminosity, by applying the selection criteria of the SDSS survey to our simulations instead of correcting the observations for incompleteness. Using this approach we again find good agreement for both the luminosity and radial distributions of MW satellites. We investigate which physical processes in our models are responsible for shaping the predicted satellite LF, and find that tidal destruction, suppression of gas infall by a photo-ionizing background, and supernova feedback all make important contributions. We conclude that the number and luminosity of Milky Way satellites can be naturally accounted for within the (Λ)Cold Dark Matter paradigm, and this should no longer be considered a problem.

Key words: galaxies: haloes – cosmology:theory, dark matter, gravitation – methods: numerical, N-body simulation

1 INTRODUCTION

The Milky Way environment provides an excellent laboratory for astrophysics. It has been used extensively in the past decades to test theoretical models of galaxy formation. In particular, the number density of satellites around our Galaxy has long been considered one of the major problems for the otherwise quite successful Λ CDM paradigm.

About a decade ago, N-body simulations attained sufficient dynamic range to reveal that in CDM models, all

haloes should contain a large number of embedded subhaloes that survive the collapse and virialization of the parent structure (Klypin et al. 1999; Moore et al. 1999 and more recently Diemand et al. 2007). Although the predicted number of substructures was in reasonable agreement with observed luminosity functions in cluster sized haloes, in Milky Way sized haloes the number of predicted subhaloes exceeded the number of observed satellites by at least an order of magnitude: the known satellite population at that time consisted of about 40 satellites with $V_c \gtrsim 20$ km/s in the Local Group (e.g. Mateo 1998), while the simulations predicted

* maccio@mpia.de

about 300 sub-haloes with $V_c \gtrsim 20$ km/s (Klypin et al. 1999; Moore et al. 1999).

Several astrophysical solutions to this problem have been proposed. Many authors have pointed out that accretion of gas into low-mass haloes and subsequent star formation is inefficient in the presence of a strong photoionizing background, as this background radiation raises the entropy of the gas, preventing it from accreting onto small dark matter haloes and lengthening the cooling time of that gas which has accreted (e.g. Babul & Rees 1992; Efstathiou 1992; Thoul & Weinberg 1996; Quinn, Katz, & Efstathiou 1996). Several studies showed quantitatively that this suppression of gas infall by cosmic reionization could plausibly reconcile the observed and predicted numbers of “classical” Local Group satellites (Bullock et al. 2000, Somerville 2002, Ricotti, Gnedin & Shull 2002, Benson et al. 2002, Read et al. 2006). It was also pointed out that tidal stripping and heating as satellites orbited in the potential of the larger galaxy could cause dramatic mass loss, even decreasing the circular velocity in the inner parts of the sub-halo (Kravtsov, Gnedin & Klypin 2004; Taylor & Babul 2004; Zentner et al. 2005). Thus many Local Group satellites may inhabit dark matter (sub-)haloes that are much less massive than they were at the time that they were accreted by their host halo.

In recent years the Sloan Digital Sky Survey (SDSS: Adelman-McCarthy et al. 2008) has changed our view of the Milky Way and its environment. The SDSS has made it possible to carry out a systematic survey for satellite galaxies, which are detectable through their resolved stellar populations down to extremely low surface brightness. As a result the number of known dwarf spheroidals has doubled in the recent past (e.g. Willman et al. 2005, Zucker et al. 2006; Belokurov et al. 2007; Irwin et al. 2007, Gilmore et al. 2007). Spectroscopic surveys subsequently measured the velocity dispersions of these systems, and confirmed their galactic nature (Martin et al. 2007, Simon & Geha 2007). This recently discovered population of ultra faint satellites has posed new challenges for models of galaxy formation and opened the possibility to test the Λ CDM paradigm at very small mass scales (e.g. Strigari et al. 2008, Macciò et al. 2009).

These new observations have made it possible to probe the faint end of the luminosity function of Milky Way satellites, down to luminosities as faint as $100 L_\odot$. Moreover the homogeneous sky coverage of the SDSS enables a robust determination of the detection limits for faint satellites. Koposov et al. (2008) provided the first determination of the volume corrected Milky Way satellite luminosity function down to these extremely faint limits, by assuming various simple radial distribution functions for the satellite population and applying the SDSS detection limits.

In light of the discovery of the new ultra-faint dwarf population and the improvements in the numerical modelling of galaxy formation, it is now timely to revisit the issue of whether the basic properties of satellite galaxies around the Milky Way, such as their number density, radial distribution, and mass-to-light ratios, can be reproduced within current cosmological Λ CDM-based models. It is also interesting to ask what physical processes might plausibly give rise to this population of extremely low-luminosity galaxies.

In this paper we combine merger trees extracted from very high resolution N-body simulations with three differ-

ent semi-analytic model (SAM) codes. These merger trees describe the hierarchical assembly of a Milky Way-like halo, while the SAMs are used to predict the relationship between the dark matter (sub)haloes and observable galaxy properties, allowing us to make a direct and detailed comparison with observational data.

The goal of this work is not only to test whether the observed properties of Milky Way satellites, including the recently discovered faint population, can be reproduced within the Λ CDM model, but also to understand how and when this extreme population formed. We aim to understand how various mechanisms (such as SN feedback, cosmic photoionization, and tidal stripping) may shape the luminosities of galaxies populating low mass dark matter substructures orbiting around Milky Way-like galaxies.

The remainder of this paper is organized as follows. In Section 2 we describe the numerical simulations. In Section 3 we briefly summarize the SAMs used in our study, highlighting the differences among the models. Section 4 contains a detailed description of the observational data used in this work. In Section 5 we compare the luminosity function, and radial distribution of simulated satellites with observational data. Finally in Section 6 we present our main conclusions.

2 SIMULATIONS

The N-body simulations of this study were obtained using PKDGRAV, a treecode written by Joachim Stadel and Thomas Quinn (Stadel 2001). The initial conditions are generated with the GRAFIC2 package (Bertschinger 2001). The starting redshift z_i is set to the time when the standard deviation of the smallest density fluctuations resolved within the simulation box reaches 0.2 (the smallest scale resolved within the initial conditions is defined as twice the intra-particle distance). The cosmological parameters are chosen to be: $\Omega_\Lambda=0.732$, $\Omega_m=0.268$, $\Omega_b=0.044$, $h=0.71$ and $\sigma_8=0.9$, and are in reasonable agreement with the recent WMAP mission results (Komatsu et al. 2009).

We selected four candidate haloes with a mass similar to the mass of our Galaxy ($M \sim 10^{12} M_\odot$) from an existing low resolution dark matter simulation (300^3 particles within 90 Mpc) and re-simulated them at higher resolution. Our high resolution haloes all have a quiet merging history with no major merger after $z=2$, and thus are likely to host a disk galaxy at the present time (with the exception of G3, which we discuss further below). The standard high resolution runs are 12^3 times more resolved in mass than the initial simulation: the dark matter particle mass is $m_d = 4.16 \times 10^5 h^{-1} M_\odot$, where each dark matter particle has a spline gravitational softening of $355 h^{-1}$ pc. Some of the main properties of the re-simulated haloes are listed in Table 1. One of the haloes, namely G3, has a mass greater than the expected mass of the MW and has experienced a major merger at $z=1.5$ so it is likely to host an elliptical galaxy. In order to check possible resolution effects (especially in the construction of the merger tree) we re-simulated one of the haloes (namely G1) with higher resolution (27^3 times with respect to the low resolution), with more than 32 million particles within the virial radius (G1_{HR} in Table 1), reaching a dark matter particle mass of $m = 3.65 \times 10^4 h^{-1} M_\odot$.

For the purpose of constructing accurate merger trees

Table 1. Dark Matter Halo parameters

Halo	Mass ($10^{12} h^{-1} M_{\odot}$)	N_{part} (10^6)	R_{vir} (kpc/h)	V_{circ} (km/s)
G0	0.88	2.12	197	178
G1	1.22	2.93	219	188
G2	1.30	3.12	250	203
G3	2.63	5.64	268	236
G1 _{HR}	1.15	31.5	211	184

for each simulated halo, we analyse 53 output times between $z = 20$ and $z = 0$. For each snapshot, we look for all the virialized isolated haloes within the high resolution region using a Spherical Overdensity (SO) algorithm. We use a time varying virial density contrast determined using the fitting formula presented in Mainini et al. (2003). We include in the halo catalogue all the haloes with more than 100 particles (see Macciò et al. 2007, 2008 for further details on our halo finding algorithm). Our procedure to construct merger trees is described in detail in Macciò, Kang & Moore (2009). We used all particles within 1.5 times the virial radius of a given “root” halo at $z = 0$ and then track them back to the previous output time. We then make a list of all haloes at that earlier output time containing marked particles, recording the number of marked particles contained in each one. We use the two criteria suggested in Wechsler et al. (2002) for halo 1 at one output time to be labeled a “progenitor” of halo 2 at the subsequent output time. In our language, halo 2 will then be labeled as a “descendant” of halo 1 if i) more than 50% of the particles in halo 1 end up in halo 2 or if ii) more than 75% of halo 1 particles that end up in any halo at time step 2 end up in halo 2 (this second criterion is mainly relevant during major mergers). Thus a halo can have only one descendant but there is no limit to the number of progenitors. On average there are 20,000 progenitors for haloes G0-G3, while the number of progenitors for the G1_{HR} run is close to 100,000.

In order to identify subhalos in our simulation we have run the MPI+OpenMP hybrid halo finder AHF (AMIGA halo finder, to be downloaded freely from <http://www.popia.ft.uam.es/AMIGA>) described in detail in Knollmann & Knebe (2009). AHF locates local overdensities in an adaptively smoothed density field as prospective halo centres. The local potential minima are computed for each of these density peaks and the gravitationally bound particles are determined. Only peaks with at least 50 bound particles are considered as haloes and retained for further analysis. As subhaloes are embedded within their respective host halo, their own density profile usually shows a characteristic upturn at a radius $r_t \lesssim r_{\text{vir}}$, where r_{vir} would be their actual (virial) radius if they were found in isolation. We use this “truncation radius” r_t as the outer edge of the subhalos and hence (sub-)halo properties (i.e. mass) are calculated using the gravitationally bound particles inside r_t .

3 SEMI-ANALYTIC MODELS

We make use of three different semi-analytic model (SAM) codes in order to predict the observable properties of galax-

ies that inhabit the dark matter haloes and sub-haloes identified in the N -body simulations described above (see Baugh 2006 for a recent review on the semi-analytic approach). We will consider predictions from the most recent implementations of three different SAMs, developed independently by different groups: (i) the Kang et al. (2005) model that has been recently updated in Kang (2008, K08 hereafter); (ii) the fiducial model of Somerville et al. (2008, S08 hereafter), which builds on the original formulation presented in Somerville & Primack (1999) and Somerville et al. (2001); (iii) MORGANA, first presented in Monaco, Fontanot & Taffoni (2007) and then updated in Lo Faro et al. (2009). Since all SAMs assume that DM haloes are the sites where galaxy formation takes place and they need a proper description of their assembly history, we will use the four merger trees extracted from N -body simulations of the G0-G3 haloes (see section 2) as a common input. In order to increase the statistical robustness of our results, in sec. 5.2 we also consider a larger set of realizations of merger trees obtained using the extended Press-Schechter (EPS) formalism (e.g. Somerville & Kolatt 1999, Parkinson et al. 2008) for K08 and S08 and the lagrangian code PINOCCHIO (Monaco et al. 2002) for MORGANA.

All the SAMs considered in this work parametrize in different ways the main physical processes acting on the baryonic component, such as atomic cooling, cosmic reionization, star formation, supernovae feedback, metal production and dust attenuation. For sake of simplicity, we will discuss here only those processes relevant in shaping the LF of MW satellites. We refer the reader to the original works for a more detailed discussion on the modeling of physical processes (see also Fontanot et al. 2009, for a comparison between different SAMs).

Although our simulations resolve subhaloes¹ we do not record the fate of subhaloes in our merger trees or make use of this information in the SAMs. When a subhalo is accreted, its position is initially either set equal to the virial radius of the parent halo at that time (K08 and S08), or extracted from a suitable distribution of radial distances (MORGANA). Moreover the orbital parameters (velocity and orbit eccentricity) for each infalling satellite are randomly selected from a distribution motivated by the statistics of satellite orbits in cosmological simulations. The dynamical evolution (and so the survival probability) of each subhalo is then computed by estimating the time required for the subhalo to lose all of its orbital energy due to dynamical friction against the background DM potential (using updated variants of the classical Chandrasekhar formula).

Each of the models that we have considered applies a different set of criteria to determine when satellites are destroyed by tidal stripping. In the K08 models, a subhalo is considered to be tidally destroyed if it either loses more than 98% of its mass (e.g. Penarrubia et al. 2008) or if its mass falls below $6.5 \times 10^6 M_{\odot}$, which is the minimum mass observed for Milky Way satellites (Strigari et al. 2008). In the S08 model, satellites are considered to be tidally destroyed

¹ From this point on, we refer to the DM haloes living within the virial radius of larger haloes as “substructure” or “subhaloes”, while we refer to the all the galaxies except the central galaxy of the larger halo as “satellites”.

when their stripped mass drops below the mass contained within a fixed fraction of the halo’s original NFW (Navarro, Frenk and White 1997) scale radius r_s (following Zentner & Bullock 2003 and Taylor & Babul 2004). In MORGANA, the tidal radius is computed at the first periastron of the satellite orbit by computing the radius at which the density of the unperturbed satellite is equal to the density of the main DM halo at the periastron. All the mass (whether dark, stellar, or gaseous) external to the tidal radius (i.e. at a lower density) is then considered unbound. The MORGANA estimates of the radii of the bulge and disk components, plus assumed density profiles for the stars and gas, are used to estimate the fraction of the baryonic mass that lies outside the tidal radius.

In all three models the effect of reionization is expressed in terms of a “filtering mass” (e.g. Gnedin 2000). This filtering mass corresponds to the mass at which haloes will only be able to accrete half of the universal baryonic content. The fraction of baryons that can be accreted as hot gas is parameterized using the following expression (Gnedin 200):

$$f_{b,acc}(z, M_{vir}) = \frac{f_b}{[1 + 0.26 M_F(z)/M_{vir}]^3}, \quad (1)$$

where f_b is the universal baryon fraction and M_{vir} is the halo virial mass. The filtering mass as a function of redshift $M_F(z)$ depends on the reionization history of the Universe, and is parameterized using the fitting formulae provided by Kravtsov et al. (2004, but see section 5.4.1).

Massive stars and supernovae may impart thermal and kinetic energy to the cold interstellar medium: in the K08 and S08 models, the rate of reheating of cold gas due to supernova feedback is given by an expression of the form:

$$\dot{m}_{rh} = \epsilon_0^{SN} \left(\frac{V_{disk}}{V_0} \right)^{\alpha_{rh}} \dot{m}_* \quad (2)$$

where ϵ_0^{SN} and α_{rh} are free parameters and \dot{m}_* is the star formation rate. K08 and S08 adopt similar values of ϵ_0^{SN} and $\alpha_{rh} \sim -2$, chosen to reproduce the faint end slope of the observed $z = 0$ global galaxy luminosity function or the low-mass end of the stellar mass function. In contrast, the MORGANA model adopts a recipe based on the notion of a self-regulated feedback loop between star formation and supernovae (Monaco 2004), which roughly corresponds to $\epsilon_0^{SN} = 1$ and $\alpha_{rh} = 0$ in terms of eqn. 2. However, we find that in order to reproduce the MW satellite LF with MORGANA we need to introduce a strong dependence of the mass loading factor $\eta \equiv \dot{m}_{rh}/\dot{m}_*$ on the galaxy circular velocity² ($\alpha_{rh} = -4$). This suggests that the phenomenological scaling in eqn. 2 is a key to the success of galaxy formation models in the Λ CDM context in predicting the MW satellite LF.

It is worth noting that the ingredients of these SAMs have all been developed with much larger galaxies in mind, and the models have previously been calibrated mainly against observations of relatively luminous galaxies ($M_* \gtrsim 10^9 M_\odot$ or $M_V \lesssim -16$). It is quite unclear whether the standard semi-analytic empirical recipes for e.g. star formation or supernova feedback should apply in galaxies as tiny as the ultra-faint Milky Way dwarfs, which may form out of just

a few molecular clouds. Therefore, it is quite an interesting experiment to see how well these models perform when extended to these very different mass scales.

4 OBSERVATIONAL DATA

We test our MW models against observations by focusing on two key aspects of MW satellite galaxy properties: their luminosity and radial distributions.

For the luminosity function we use the results of Koposov et al. (2008; SK08 hereafter). SK08 recently presented a quantitative search methodology for Milky Way satellites in the SDSS DR5 data and used this method to compute detection efficiency maps, which ultimately allowed the construction of the first completeness-corrected satellite galaxy luminosity function (see also Walsh, Willman & Jergen 2009). SK08 measured the luminosity function (LF) down to $M_V = -2$, and found that it can be described by a single power law of the form $dN/dM_v = 10 \times 10^{0.1(M_V + 5)}$. At the very faint end ($M_V > -5$), in order to compute the completeness correction, a radial satellite distribution around the host must be assumed; in all the luminosity function plots presented in this paper the upper data points (always shown as open circles with no error bars) are obtained assuming an isothermal density distribution while the lower points (solid circles with error bars) are obtained assuming an NFW (Navarro, Frenk and White 1997) distribution.

We also use a reverse approach to addressing the completeness issue by performing the comparison in “observational space”. Instead of assuming a radial distribution for the observed galaxies, we apply the detection criteria of the SDSS to our simulations (see section 5.3 for more details) and compare directly with the raw data from the SDSS. For this comparison we construct a “hybrid” data set. For satellites brighter than $M_V = -9$, in order to increase the number statistics, we gather together satellites from the Milky Way and the Andromeda galaxy (data from Mateo 1998 and Metz et al. 2007), and we assign a weight of $w = 0.5$ to each satellite, assuming that current surveys are complete down to this limit. For fainter satellites we collect data from Martin, de Jong & Rix 2008 (MdJR08 hereafter) and, in order to account for the fact that the SDSS surveyed only one-fifth of the sky, we set $w = 5$ for these faint galaxies. The adopted M_V threshold for splitting the observational sample is justified by the low luminosity of all newly discovered satellites both around the Milky Way and the Andromeda galaxy (McConnachie et al. 2008).

In addition, using the same data set described above, we compute the cumulative radial distribution of satellites (i.e. the number of satellites within a given distance from the Sun). Distances for bright satellites are taken from Metz et al. (2007), while we use results compiled in MdJR08 for faint galaxies ($M_V > -9$). In computing the radial distribution we assign to each galaxy the same weight adopted for the LF.

5 RESULTS

In this section we present results for both the SAMs and numerical (dissipational and dissipationless) simulations and

² In order not to spoil the agreement of this model for $M_* > 10^9 M_\odot$ galaxies, we retain the original recipe $V_c > 100$ km/s DM halos and adopt Eqn. 2 in galaxies with $V_c < 100$ km/s.

compare them with the observational data set described in Section 4. First we compare the dynamical evolution of satellites in SAMs and in N-body simulations, and then we present results for the Luminosity Function (LF) of simulated satellites and analyze the importance of different physical processes (e.g. reionization, stellar stripping and supernova feedback) in shaping the LF. We then present results for the radial distribution and compare them with observations.

5.1 Dynamical evolution of sub-haloes in SAMs and N-body simulations

In the SAMs investigated here, we chose to make use of N-body based merger trees for “isolated” (or distinct) haloes only, and to model the dynamical evolution of satellites semi-analytically (see Section 3). Thus, there will not be a one-to-one correspondence between the masses or positions of sub-haloes at $z = 0$ in the SAMs and in the actual N-body simulations. In this section we check that the statistical distributions of subhalo masses and radii predicted by the semi-analytic models are in agreement with those of subhaloes identified in the N-body simulations. This comparison is only possible for the K08 and S08 models, since the MORGANA model does not explicitly follow the dynamics of dark matter substructures. Figure 1 shows the cumulative subhalo mass function from N-body and SAMs for our four Merger tree G0-G3. The G1_{HR} halo is shown for the K08 model only. The SAM results are obtained by averaging over ten different realizations of the random orbit selection process and are truncated at the N-body mass resolution limit. A simple way to quantify the agreement between two distributions is to perform a Kolmogorov-Smirnov (KS) test (Press et al. 1992). In the following we will quote as KS results, the probability that two distributions are drawn from the same parent population. K08 and S08 SAMs give an average KS probability of 88% and 90% respectively, when compared to the subhalo mass function from the N-body simulations, showing thus good agreement with the numerical results.

The radial distribution of satellites is a key piece of information for deciding whether a satellite will be detectable in the SDSS survey. It is therefore important to also check that the SAMs correctly predict the radial distribution of subhaloes within the parent halo. Figure 2 shows the radial number density of subhaloes (without including the central galaxy); while on average there is good agreement between SAMs and N-body results for both models (KS test results: 87% and 88% S08 and K08 respectively), there is a systematic off-set between K08 and S08, especially at distances < 100 kpc/h. The reason for this off-set resides in the different fitting formulas for tidal destruction and dynamical time implemented in the two models, but is nevertheless too small to affect our analysis.

In the semi-analytic models used here, the initial orbit eccentricity of an infalling subhalo is randomly selected from a distribution motivated by the results from cosmological N-body simulations. We checked that the scatter due to different realizations of the orbit distribution is fairly small, and mostly affects the less numerous, massive satellites which are not the focus of our study.

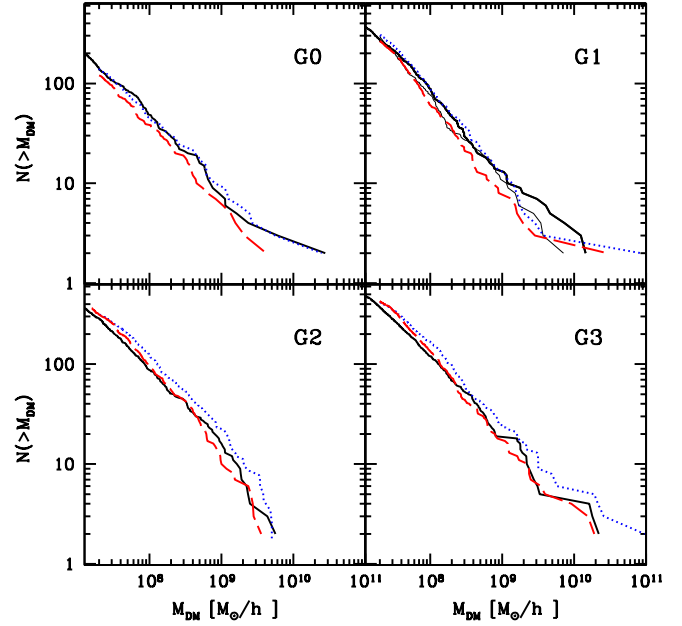


Figure 1. Comparison between the subhalo mass function at $z = 0$ (within R_{vir}) in the N-body simulations (solid black line) and the predictions from the semi-analytic models of K08 (red dashed line) and S08 (blue dotted line). Each panel shows results for a different dark matter halo. The (black) thin solid line in the G1 panel shows the results of the K08 SAM when applied to the G1_{HR} halo.

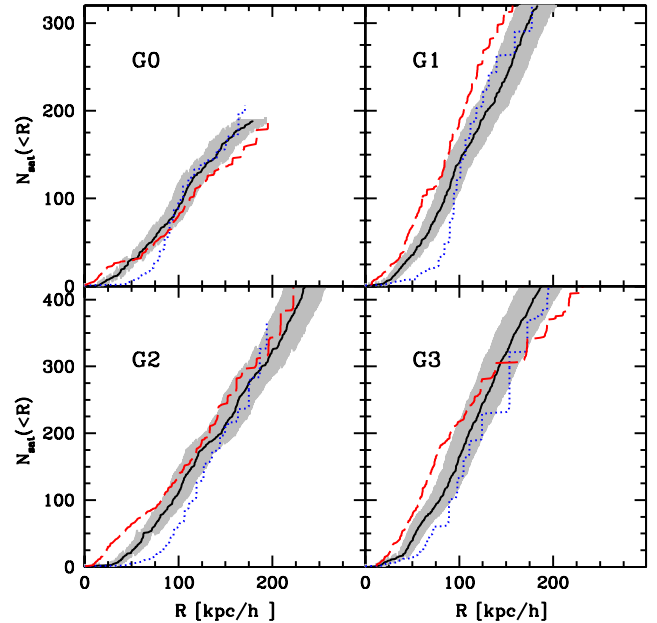


Figure 2. The cumulative number density of satellites as a function of radius from the center of the parent galaxy. The results from the N-body simulations are shown by the solid (black) line, the shaded (grey) area shows the 1σ scatter over five different realizations of the satellite orbit distribution. Results from the K08 and S08 SAMs are shown by the (red) dashed line and (blue) dotted line respectively. Each panel shows results for a different dark matter halo.

5.2 Satellite Luminosity Function

We now compute satellite LFs using the four merger trees obtained from the N-body simulations as common input for our semi-analytic models; this allows us to isolate the impact of the different physical ingredients in the SAMs because the DM halo merger histories are exactly the same in all three models. Figure 3 shows the predictions from our three SAMs, adopting $z_r = 7.5$ as the redshift of reionization. We plot all satellites within $R = 280$ kpc in order to be consistent with the SK08 data set. Solid lines show the mean of satellite distribution and the (grey) shaded area shows the 1σ Poisson scatter around that mean.

All of the models predict that the number of satellites brighter than $M_V = -3$ is of the order of ~ 100 and could easily be several hundreds (e.g. G3). This is in agreement with recent estimates of the number of observed satellites obtained by several different approaches (e.g. Tollerud et al. 2008; Madau et al. 2008; Koposov et al. 2009).

All the models show that the total number of satellite galaxies depends on the host halo mass. The LF of the G0 halo (the least massive one, see Table 1) is almost flat and has a lack of satellites at the faint end compared to the MW data. On the other hand, in the most massive halo (G3), the SAMs predict more satellite galaxies at all luminosities than are observed in the MW. This trend between halo mass and the LF does not depend on the SAM used to populate dark matter substructures and indicates that the total mass of the dark matter halo has a quite strong influence in determining the normalization (and shape) of the satellite LF.

All three semi-analytic models considered in this work are able to do a reasonably good job of reproducing the observational data. The K08 and S08 models (upper and middle panels) in figure 3 quite successfully reproduce the observed LF for satellite galaxies over the entire luminosity range $-2 \geq M_V \geq -16$. The MORGANA model (lower panels in figure 3), tends to predict slightly more satellites at intermediate luminosity ($-10 > M_V > -12$) but it is nonetheless in good agreement with the observations especially if an NFW distribution is assumed for observed satellites. In the G1 panel for the K08 model we also show the LF obtained using the G1_{HR} merger tree (dotted black line). We see that the higher resolution merger tree produces almost indistinguishable results.

In some cases, certain models and certain haloes show a dearth or even absence of the most luminous satellites (e.g. S08 and K08 G0, G2 in all models). This should not be a serious cause for concern, because the variance in the number of massive subhaloes hosting these luminous satellites is very large and depends on the detailed merger history of the halo. Moreover, the predicted number in the SAM is very sensitive to the random orbit chosen, as discussed in Section 5.1. To assess this issue in a more robust way, we need to increase the number of merger tree realizations of MW mass haloes. We do this using semi-analytic merger trees instead of the merger trees extracted from N-body simulations. For each model we generated 40 merger trees for DM haloes in the estimated mass range of the Milky Way dark matter halo, $(0.8 - 1.2) \times 10^{12} h^{-1} M_\odot$ (Klypin, Zhao & Somerville 2002). Each of the SAM codes has its own algorithm for generating merger trees: the K08 and S08 model use different implementation of the EPS algorithm, while MORGANA uses

the PINOCCHIO code. Figure 4 shows the averaged luminosity function for the three semi-analytic models (we tested that the sub-halo mass function from the EPS/PINOCCHIO trees is in agreement with the one extracted from the Nbody simulations).

The K08 and S08 model are, again, in good agreement with the observational data: they are able to fit the Milky Way luminosity function in the range $-15 < M_V < -2$ (KS test results: 90.9% for S08 and 90.5% for K08). The K08 model shows a small deficit of satellites at brighter magnitudes (especially if compared with S08 and MORGANA) but this occurs where the number of observed satellites has a large error bar due to poor number statistics. Our models produce much better agreement with the number of luminous satellites with $M_V < -15$ relative to the predictions of Benson et al. (2002). Because of the large number of differences between the Benson et al. models and those considered here, we can only speculate on the source of this difference.

It is also interesting to note that the K08 and S08 models suggest that the LF of ultra-faint satellites has a downward kink below about $M_V \sim -6$, in better agreement with the SK08 observational results adopting an NFW, rather than isothermal, radial density distribution for the satellites. An NFW distribution for satellites is predicted by hydrodynamic simulations (Macciò et al. 2006). The comparison between the MORGANA model and the observational results can only be performed down to $M_V = -5$ in this case. This because the PINOCCHIO code has never been tested on such small scales (e.g. Li et al. 2006) and we did not feel confident in using merger trees with a mass resolution below $\sim 10^8 h^{-1} M_\odot$. In the tested range for M_V the MORGANA model is also in good agreement with observations (KS test: 90.2%).

In figure 5 (lower panel) we plot the stellar mass and luminosity of galactic satellites versus their dark matter subhalo mass; results are shown for the K08 model for all haloes, and are similar for the other models. For this comparison we used both the present dark matter mass ($M_{DM}(z = 0)$) and the mass of the subhalo at the time of accretion ($M_{DM}(z_{acc})$). The difference between the two reflects the effects of tidal stripping on the dark matter substructure. The correlation between the present day dark matter mass and luminosity is quite broad and, for low luminosities, $M_{DM}(z = 0)$ at a fixed luminosity spans almost 3 orders of magnitude. This is because tidal stripping of the dark matter subhalo washes out the initial correlation between luminosity and $M_{DM}(z_{acc})$. The same applies to the comparison between the dark and stellar mass of galactic satellites, as shown in the upper panel of figure 5.

Recently, Strigari et al. (2008) pointed out that one of the curious properties of the newly discovered population of faint satellites is that over four orders of magnitude in luminosity, these objects seem to contain a nearly constant total mass within a radius of 300 pc. If we focus on the faint population in figure 5, with $-3 < M_V < -10$, we can see that the huge scatter in DM mass at fixed luminosity or stellar mass provides a partial explanation for this apparent “common” mass scale for the faint satellites. Macciò, Kang & Moore (2009, see also Li et al. 2009) investigated this in more detail, and presented a direct comparison between the predicted luminosity and the mass within 300 pc for faint satellites in our simulations. They argued that the

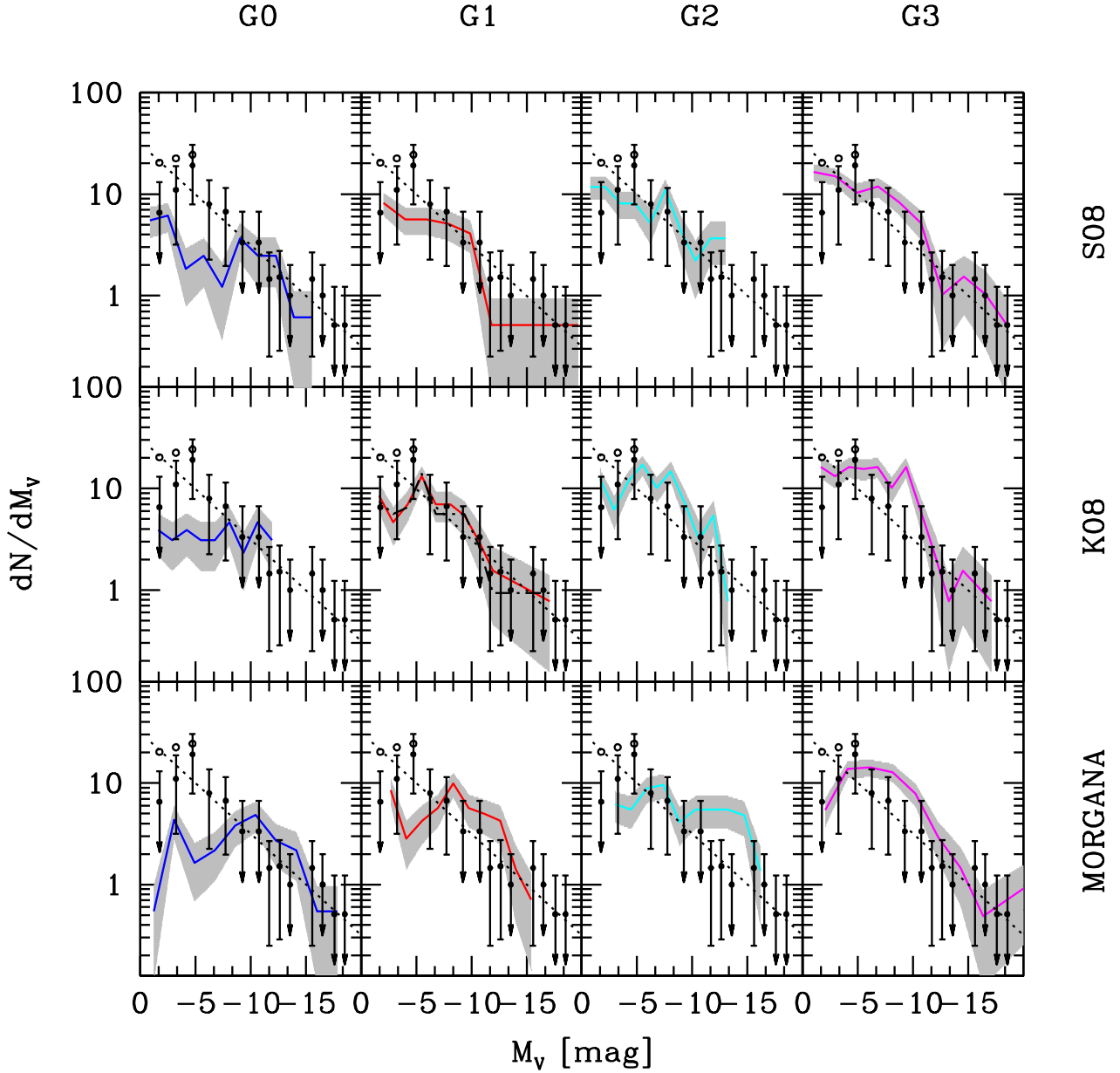


Figure 3. The Milky Way satellite luminosity function predicted by our three semi-analytic models (S08, K08 and MORGANA from top to bottom) using the G0-3 halo merger trees (from left to right), with an assumed reionization redshift $z_r = 7.5$. The median of the satellite distribution is shown by the solid line, while the shaded area represents the 1σ Poisson scatter around the mean. Observational data are taken from SK08 under the assumption of two different radial distributions of satellites, NFW-like (solid circles with error bars) and isothermal (open circles). The arrows on error bars indicate that there is only one galaxy in that particular bin, and so the Poisson error is formally 100%. The dotted line shows a single power law fit to the data: $dN/dM_v = 10 \times 10^{0.1(M_v + 5)}$. In the G1 panel of the K08 model results for the G1_{HR} run are also shown as a dashed (black) line.

inner profiles of haloes that are initially very concentrated are less effected by tidal heating than haloes that are less concentrated, so that the mass within 300 pc is reduced for more massive subhaloes (which are less concentrated) relative to less massive ones. When they corrected for this concentration-dependent modification of the inner density profile, they found that the Strigari et al. (2008) results are quantitatively reproduced by our simulations.

5.3 Luminosity Function in the Observational Plane

The luminosity function of SK08 has been determined under certain assumptions for the radial distribution of satellites around our Galaxy. It is also interesting to apply the observational selection criteria to our simulations and compare “in the observational plane”, i.e. with the *raw* data from the SDSS without completeness corrections applied. To make

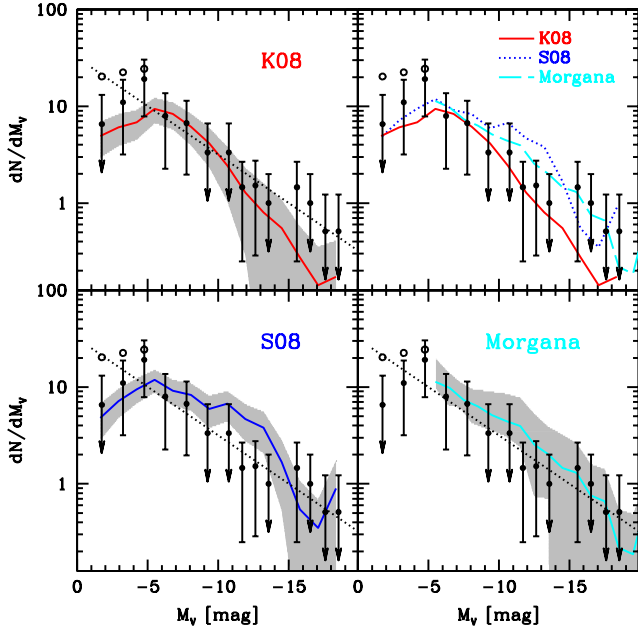


Figure 4. Satellite Luminosity function predicted by SAMs using semi-analytic merger trees (EPS and PINOCCHIO, see text for details). Symbols have the same meaning as in figure 3. The upper right panel shows the average satellite LF for the three semi-analytic models together. MORGANA results are shown only down to $M_V = -5$, due to a resolution limitation in the PINOCCHIO code; see text for more details.

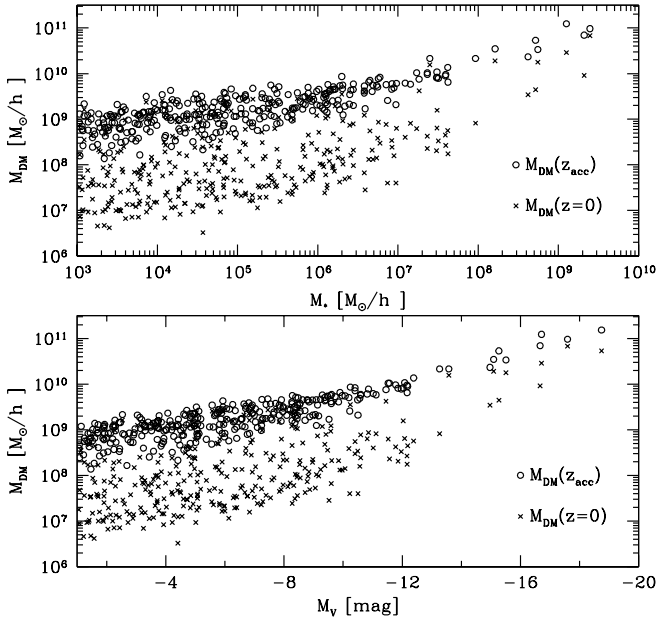


Figure 5. The dark matter mass of galaxy satellites versus their luminosity (lower panel) and stellar mass (upper panel). Open circles show the masses at time of accretion, while crosses show the present ($z=0$) dark matter mass. Results are shown for the K08 model for all haloes G0-G3.

such a comparison we have applied to our sample of satellites a *visibility* criterion, in order to determine if a given satellite would be detected in the SDSS. We assume that *all* satellites brighter than $M_V = -10$ would be visible and included in the SDSS sample. For fainter satellites, we adopt a criterion based on both satellite distance and luminosity (see SK08 for more details):

$$\log(R/\text{kpc}) < 1.04 - 0.228 \times M_V. \quad (3)$$

In the above formula the distance R is measured from the Sun and not from the center of the galaxy. In order to convert our galacto-centric distances into helio-centric distances, we assume the Sun to be located at 8 kpc from the center of the galaxy (8,0,0); moreover, since for each satellite galaxy we only know its distance from the galactic center, we randomly assign position angles (ϕ, θ) to each of them (see also Tollerud et al. 2008). We exclude from the comparison galaxies more distant than 280 kpc. Moreover since the SDSS covers only approximately one fifth of the sky we randomly select 1/5 of our satellites. We then average over 100 different realizations of this random sampling. Observational data for the recently discovered SDSS satellites are taken from MdJR08. Figure 6 shows the comparison between the observations and the luminosity functions obtained with the K08 model (the S08 model gives very similar results and this comparison is not possible for the MORGANA model, because it does not provide the distance of satellite galaxies from the main halo). The direct comparison with the observational data confirms our previous results on the luminosity function. Our models are able to reproduce the data for haloes G0-G2, while halo G3 slightly overproduces the number of faint satellites. The agreement between the data and models implies that the distance-luminosity relation of our satellites is similar to the observed one.

The application of the selection criteria of the SDSS to our simulated data also allows us to compare the radial number density of satellites in our models *vs* observations. Results are shown in figure 7. From this figure we see that our simulations reproduce both the observed slope and normalization of the satellite radial distribution for G0 and G2 (KS test results: 96% and 91%) while the agreement is less good for G1 and G3 (KS: 76% and 77%). The difference for G3 can be ascribed to the overall higher visible satellite number (e.g. fig. 3). One possible explanation for G1 can be related to its higher formation redshift (half mass in place) than the other two galaxies. This implies that subhaloes will have, on average a higher accretion redshift, and thus have more time to sink to the center.

Finally in figure 8 we compare the radial distribution of DM substructures and “observable” satellites in the K08 model (obviously, observability depends on many factors, but in this context we simply consider all satellites with $M_V < -1$ to be “observable”). In the upper panel we show the number density radial distribution of all “observable” satellites ($M_V < -1$), of faint satellites ($-9 < M_V < -1$) and of classical satellites ($M_V < -9$). The number-weighted distribution of observable satellites (which are dominated by the much more numerous faint population) traces the subhalo distribution (but is down by a factor of ~ 2) at small radii (within $R/R_{\text{vir}} \approx 0.2$), but flattens relative to the subhalo distribution at large radii. This implies that “observable” sub-haloes are more concentrated near the large galaxy

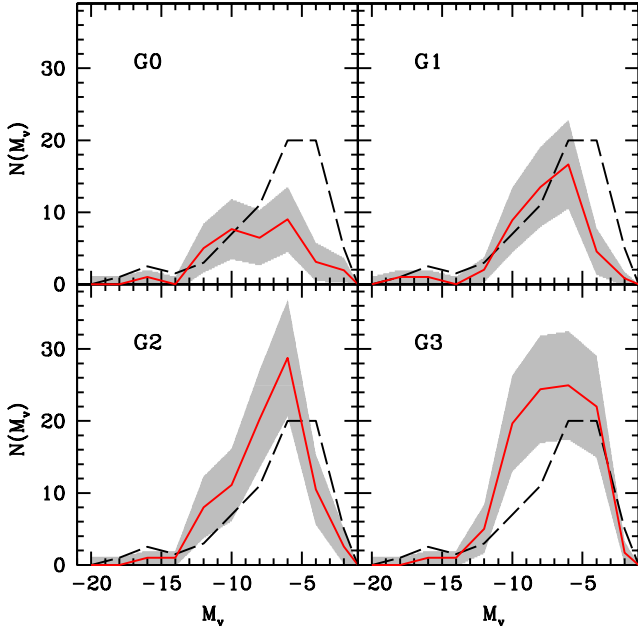


Figure 6. Comparison between the “raw” SDSS data (uncorrected for completeness) and model predictions with the SDSS visibility criteria applied to the simulations (see text for details). The observational data are shown by the (black) dashed line, the K08 model is shown by the solid (red) line, and the shaded area shows the 1σ Poisson scatter around the mean value.

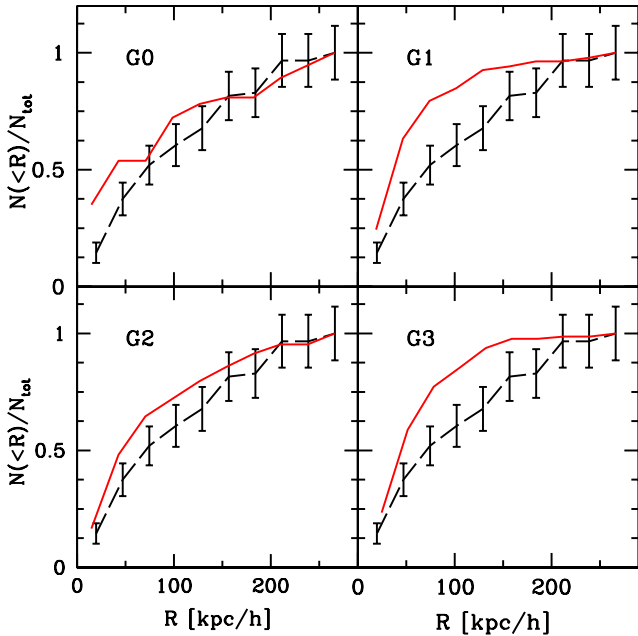


Figure 7. The fraction of satellites as a function of the distance from the central galaxy. Observational data are shown by the (black) dashed line with error bars (representing the Poisson noise). The K08 model is shown by the solid (red) line.

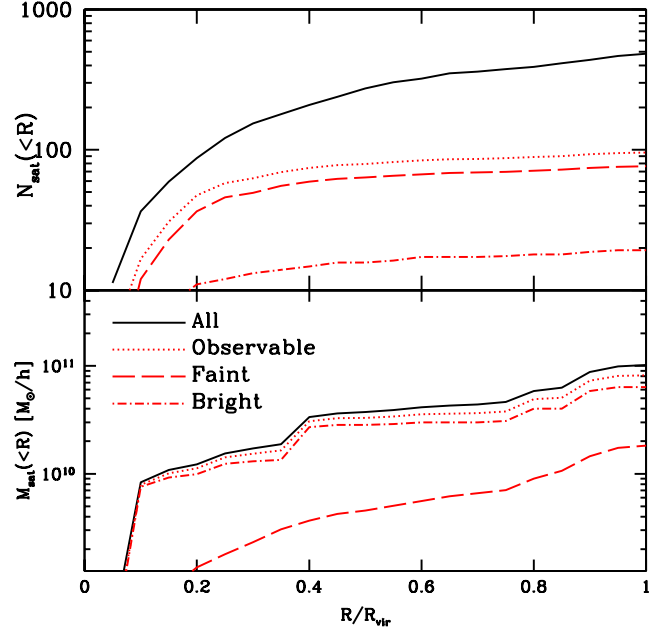


Figure 8. Upper panels: number-weighted cumulative fractional radial distribution of satellites; the black line shows all substructures (dark and observable), the (red) dotted, dashed and dot-dashed lines are for the “observable” satellites ($M_V < -1$), the faint satellites ($-9 < M_V < -1$) and the classical satellites ($M_V < -9$), respectively. Lower panel: same as upper panels but with weighted by satellite mass. The results were obtained by averaging over the four haloes G0-G3; only the K08 model is shown.

than the overall population of subhaloes (see also Kravtsov et al. 2004). When satellites are weighted by their mass (lower panel of the same figure), the distribution is dominated by the classical (bright) satellites, and is almost identical to the mass-weighted distribution for all sub-haloes. Thus, the different radial distribution of “observable” and dark satellites is due to the suppression of star formation in low-mass haloes due to cosmic reionization and feedback processes.

5.4 Physical Processes that Shape the Satellite Luminosity Function

We have shown that it is indeed possible to reproduce the observed Milky Way satellite luminosity function within the Λ CDM model; we now investigate the role of various physical processes in shaping the LF in our theoretical models, with a focus on the origin of the newly discovered ultra-faint satellite population. There are several possible physical origins for the ultra-faint satellite population: it can originate from (i) object that formed in haloes with $T < 10^4$ K via H_2 cooling (e.g. Salvadori & Ferrara 2009); (ii) haloes with $T > 10^4$ K that were inefficient at accreting (hot) gas, because of photoionization; (iii) haloes with $T > 10^4$ K in which star formation was inefficient because of strong supernova feedback; (iv) objects that originally had larger stellar masses but have experienced significant stellar stripping.

In the following sections we will investigate scenarios (ii)-(iv). The first scenario, in which the ultra-faint dwarfs form via H_2 cooling in haloes with $T < 10^4$ K, is not ac-

counted for in our models. It is likely however that some ultra-faint satellites could form in this way, and this could help in explaining the small gap between the theoretical predictions and observations for $M_V \gtrsim -3$ (e.g. figure 4).

5.4.1 Reionization

We test the effect of our adopted parametrization of cosmic reionization on our results, by both varying the reionization redshift within our reference model based on Kravtsov et al. (2004) and by applying a simple modification to this model to take into account recent results based on high resolution hydrodynamical simulations (e.g. Okamoto et al. 2008; Hoeft et al. 2006).

The redshift at which reionization occurs is still quite uncertain, but it is bracketed in the range $7 < z_r < 15$ (3σ range from Komatsu et al. 2009); moreover, due to the fact that reionization proceeds in an inhomogeneous way, the actual redshift of reionization for the Local Group could substantially differ from the average reionization redshift of the Universe (Weinmann et al. 2007). Figure 9 shows the impact of varying the reionization redshift on the G1 luminosity function for the K08 model using the standard reionization parametrization (S08 and MORGANA show a similar trend). Without any suppression of gas accretion due to reionization, the simulated LF contains too few satellites fainter than $M_V = -5$ and too many with $M_V \sim -9$. This is because, in absence of reionization, hot gas can cool very efficiently via atomic cooling, and every halo can transform a large fraction of its gas content into stars before SN feedback shuts star formation down. When the effect of reionization is taken into account, the amount of gas available for cooling and star formation is reduced in low mass haloes, and many galaxies are shifted from intermediate luminosities ($-15 < M_V < -6$) to low luminosities ($M_V > -6$), producing a luminosity function that is close to a power-law and is in good agreement with the data. It is also interesting to note that the LF is almost insensitive to the redshift of reionization (solid line shows results for $z_r = 7.5$, dashed line for $z_r = 17$); this is in agreement with earlier results obtained by Kravtsov et al. (2004).

In addition to uncertainty about the redshift of reionization, there is still a debate about the value of the characteristic mass, M_F , below which galaxies are strongly affected by photoionization. Okamoto et al. (2008, see also Hoeft et al. 2006), using hydrodynamical simulations, recently suggested that the actual value of M_F can be significantly lower than values previously obtained (e.g. by Gnedin 2000). In order to explore the implications of their results, we introduce a factor γ that multiplies the original value of $M_F(z)$ as derived by Gnedin (2000, see eq. 1). We have used two constant values for γ , namely 0.2 and 0.5, and a redshift dependent expression $\gamma(z) = (1+z)^{1.1}/11.8$, derived from figure B1 of Okamoto et al. (2008). The results for these three modified models are shown in figure 10 for the G1 halo and for the K08 model (results from the other models are similar). We see that the reduced value of M_F has the effect of increasing the number of galaxies with $M_V \sim 10$, creating a bump in the LF, with respect to the standard case, similar to what we saw in figure 9 for the no reionization run (dotted line). This is true especially for strong suppression of photo-ionization as in the $\gamma = 0.2$ and $\gamma(z)$ cases. Nev-

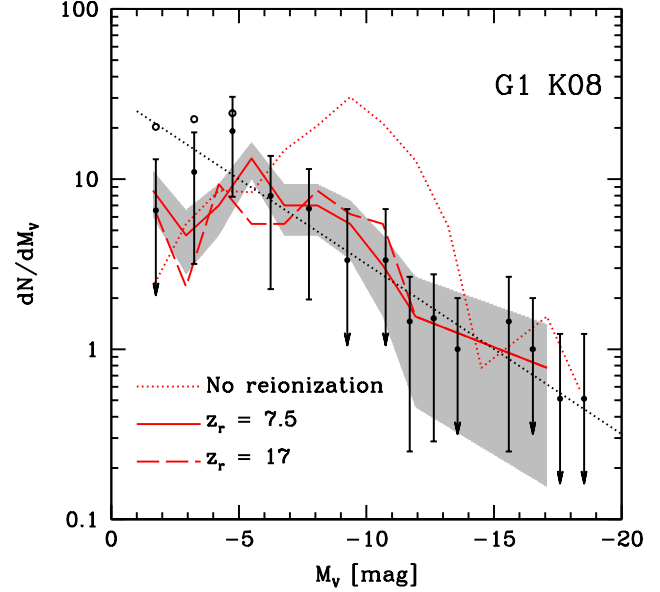


Figure 9. Satellite luminosity function of the G1 halo in the K08 model for three different reionization redshifts. The solid line represents our fiducial model with $z_r = 7.5$, the dashed line is for $z_r = 17$, and the dotted line is for a model with no reionization (but including all other kinds of feedback). The shaded area represents the 1σ scatter around the mean of the $z_r = 7.5$ model.

ertheless it is still possible to reconcile the simulated LFs with the observational data by increasing the reionization redshift, as shown in the right panel of figure 10, where we use $z_r = 11$.

In summary, it is interesting to note the interplay between the strength of the suppression of gas accretion due to photo-ionization (as reflected in the filtering mass scale) and the redshift of reionization. In our standard models, in which the suppression is relatively strong (M_F is large), we find a weak dependence of the predicted LF on the adopted value of the reionization redshift, while in models with a lower overall normalization of the filtering mass, we find a stronger dependence on the redshift of reionization.

5.4.2 Stellar Stripping and Tidal Destruction

In our models, we distinguish between “stellar stripping” and “tidal destruction”. In the former, we track the amount of *stellar* material that is stripped from the galaxy as it orbits within the parent halo. In the latter, we assume that a satellite’s baryonic mass is unaffected until its total mass is stripped by a critical amount, at which point the satellite is simply removed. Obviously, these are aspects of the same physical process and it is somewhat artificial to distinguish between them. We do so simply to illustrate the sensitivity of our results to different implementations of this physical process in models.

The MORGANA model allows for the modelling of stellar stripping as a satellite galaxy orbits around the parent galaxy (see section 3 for more details), while the K08 and S08 models assume that the stellar content of a satellite

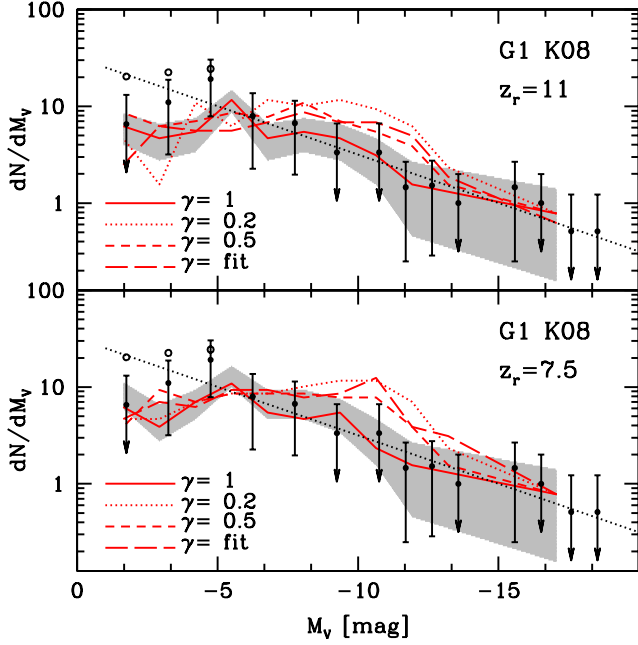


Figure 10. Satellite luminosity function for the G1 halo in the K08 model, for different parametrizations of cosmic reionization. The solid line shows results for the standard reionization model ($\gamma = 1$, see text for the definition of γ) based on Kravtsov et al. (2004). The dotted and short dashed lines show results for a filtering mass M_F reduced by 80% and 50% respectively. The long dashed line is for a model with a redshift dependent expression for the modification of M_F (see text for more details). The shaded area represents the 1σ scatter around the mean of the $\gamma = 1$ model. The left upper and lower panels are for $z_r = 11$ and 7.5 respectively.

remains unchanged until the dark matter halo is stripped beyond a certain critical point, at which point the galaxy is destroyed completely.

First we investigate the possible effect of stellar stripping on the predicted satellite LF using the MORGANA code. We compare three different MORGANA runs with no, standard (moderate) and high stellar stripping; this latter case is obtained by increasing by a factor of three the fraction of stripped stellar mass with respect to the standard run (i.e. we remove from the satellites three times the mass that is beyond the tidal radius). Results for the luminosity function are shown in figure 11. In the case of standard stripping the average stripped stellar mass is of the order 5% – 10% with no mass dependence. Comparing the LF of this case with the no-stripping case, it appears that stellar stripping is almost negligible for satellites brighter than $M_V = -5$ and it marginally affects fainter satellites. When the strength of the stellar stripping is increased the mass loss is, of course, more important and as much as 40% of the stellar mass can be stripped, with a strong dependence on the orbital parameters. However, even in this case the overall effect on the LF is relatively small. According to these results, stellar stripping is not one of the most important processes that shapes the satellite LF or produces ultra-faint satellites.

On the other hand we find that the modelling of tidal destruction of satellites does have a significant effect on the satellite LF. If we neglect tidal destruction, we find many more low-mass subhaloes than are seen in the N-body simu-

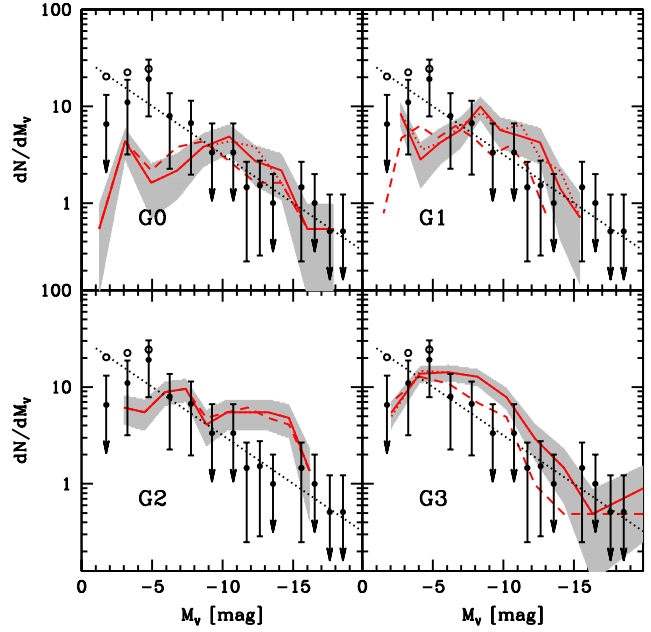


Figure 11. The effect of stellar stripping on the satellite luminosity function. Results from the MORGANA model are shown for different levels of stellar stripping (no stripping, standard, and high). The solid line shows the moderate (standard) stripping case (as shown in figure 3); dotted and dashed lines show the no-stripping and strong stripping models respectively.

lations, and we would also predict many more faint satellites than are observed in the MW. Following Zentner & Bullock (2003) and Taylor & Babul (2004), the S08 model considers a satellite to be tidally destroyed when the mass of the dark matter sub-halo has been stripped to a value less than or equal to the mass within $f_{\text{dis}} r_s$, where r_s is the halo’s original NFW scale radius. Zentner & Bullock (2003) adopt $f_{\text{dis}} = 1$ while Taylor & Babul (2004) adopt $f_{\text{dis}} = 0.1$. Figure 12 shows the effect of varying the parameter f_{dis} in the S08 model; we see that this can change the number of faint satellites by as much as a factor of ten. We find good agreement with the observed MW satellite LF for $f_{\text{dis}} \sim 0.1 - 0.5$.

5.4.3 Supernova Feedback

Feedback from supernovae is believed to be an important mechanism for regulating star formation in low mass galaxies, and it plays a primary role in shaping the LF in semi-analytic models. It is then important to disentangle its effect from the effect of cosmic reionization discussed in the previous section. To investigate this, we first compare our reference model with both cosmic reionization and SN feedback, and a run with only cosmic reionization (no SN feedback). The results for the K08 model are shown in figure 13; the S08 model shows similar behaviour. In the absence of stellar feedback, the SAM predicts a deficit of faint satellites ($M_V > -5$) and an overabundance of intermediate luminosity satellites ($-15 < M_V < -10$) when compared with the observations. The inclusion of SN-driven outflows again moves intermediate luminosity galaxies into the ultra-faint regime by removing a significant fraction of the gas and thereby suppressing star formation.

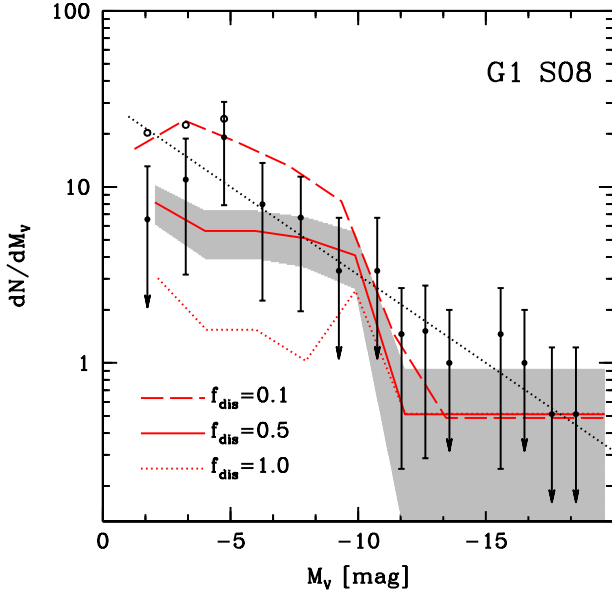


Figure 12. The effect of varying the tidal destruction parameter f_{dis} (see text) on the predicted MW satellite LF in the S08 model, for the G1 halo.

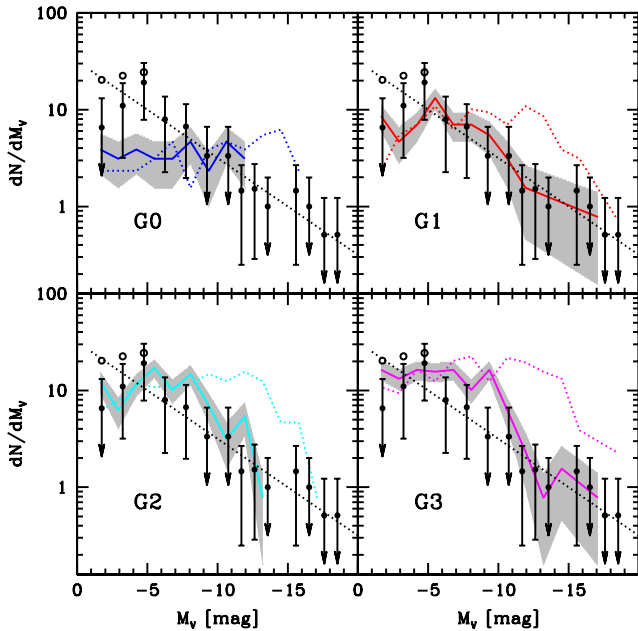


Figure 13. The effect of supernova feedback on the satellite luminosity function. Results from the K08 model with SN feedback switched *on* (solid line with shaded area) and *off* (dotted line) are shown.

As we already discussed in Sec. 3 the original version of the MORGANA model, implementing a recipe for supernova feedback derived from Monaco (2004), does not produce good agreement with the MW satellite LF. In order to reproduce the observed MW satellite LF, we found it

necessary to modify the stellar feedback modeling using an approach similar to K08 and S08.

We conclude that strongly *differential* SN feedback (in which the outflow rate relative to the star formation rate is much higher in low-mass galaxies) plays a key role in reproducing the MW satellite LF in these models.

5.4.4 Satellite Strangulation

There is another effect that in our models can cause relatively high-mass haloes ($T > 10^4\text{K}$) to be inefficient at forming stars and thus to produce ultra-faint satellites. This effect is a result of the fairly standard assumption in SAMs of “satellite strangulation”, namely that the hot gas halo that could provide new gas to a galaxy is stripped immediately when a galaxy becomes a satellite in a larger halo. Thus, haloes that are accreted by the parent halo soon after they crossed the threshold for atomic cooling ($T > 10^4\text{K}$) and thereafter are starved of any new gas cooling or accretion can have very low stellar masses.

In order to explore the importance of this effect, we look for a correlation between satellite luminosity and the timescale τ_S , which we define as:

$$\tau_S = \frac{t_{\text{acc}} - t_{\text{form}}}{t_{\text{cool}}} \quad (4)$$

where the formation time (t_{form}) is defined as the time at which the halo reaches a virial temperature $T > 10^4\text{K}$ and can first begin to cool, t_{acc} is the time at which the galaxy is accreted by the parent halo and becomes a satellite, and the cooling time (t_{cool}) is the time needed for the gas to radiate away all of its energy via atomic cooling, computed at $z = z_{\text{acc}}$ (the standard definition of cooling time used in SAMs). Satellites with $\tau_S < 1$ may have been “strangulated” before they were able to cool a significant fraction of their gas. Figure 14 shows that some (about 15 %) of the faint satellites have $\tau_S < 1$ and therefore may have been impacted in part by this effect (though photo-ionization and SN feedback may still play a role in these objects as well).

6 DISCUSSION AND CONCLUSIONS

In the last few years, a new population of ultra-faint dwarf satellite galaxies has been discovered around our Galaxy. Given these new observational data, it is timely to revisit the long standing problem of the number of satellites around Milky Way-like dark matter haloes as predicted in the ΛCDM scenario. We address this issue by combining high resolution N-body simulations with three different semi-analytic models of galaxy formation. Four high resolution N-body simulations are used to create detailed merger trees that represent the assembly history of a Galactic dark matter halo. These merger trees are then used as common input for three SAMs for galaxy formation, namely the MORGANA model (Monaco et al. 2007), the Somerville et al. model (S08, Somerville et al. 2008) and the Kang et al. model (K08, Kang et al. 2008), to study the expected abundance and properties of satellite galaxies in the Local Group.

Because the SAMs do not use the explicit information

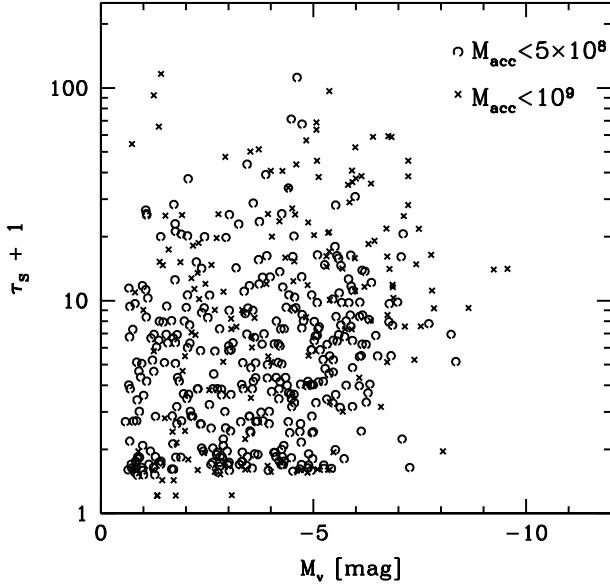


Figure 14. Relation between satellite luminosity and τ_S (defined according to eq.4) for the K08 model. Different symbols show different values for the total mass of the satellite at the time of accretion, as indicated in the figure label. Satellites with $\tau_S < 1$ may have been affected by “strangulation”.

about subhaloes from the N-body, but track subhalo evolution using semi-analytic recipes, we first compare the mass function and radial distribution of dark matter subhaloes predicted by the SAMs with the results directly obtained from the N-body simulations. We find that the parameterizations of subhalo merging and tidal stripping and destruction adopted by the S08 and K08 models are able to fairly accurately reproduce simulation results for the mass distribution and radial distribution of satellites.

We then test the luminosity function of our simulated satellite population against the latest observational results for the MW satellite luminosity function. Our models are all able to reproduce the LF down to a magnitude $M_V = -5$; at fainter magnitudes ($-5 < M_V < -1$) the K08 and S08 models also provide a good fit to the observational data, while the MORGANA model tends to underestimate the abundance of ultra-faint satellites, though the predictions are still consistent with the MW data at the $1\text{-}\sigma$ level. All models seem to suggest a decrease in the satellite number density below $M_V \sim -5$, consistent with the assumption of a NFW like radial distribution for observed satellites.

We also perform the comparison between our model predictions and the observations in the “observational plane”, i.e., by applying “visibility” criteria to the simulated satellites and comparing with the SDSS data without any completeness corrections applied. In this case, instead of assuming a radial distribution for the observed satellites (which could in principle depend on e.g. satellite mass or luminosity in a complex way), we make use of the predictions of our models for the joint distribution function of satellite luminosity and distance from the central galaxy. We again find good agreement, increasing the robustness of our results.

We investigated the main physical processes responsible for shaping the luminosity function of Milky Way satellites in our models. In the absence of cooling by molecular hydrogen, and in the absence of processes like photo-ionization, SN feedback, or stellar stripping, the predicted satellite LF would show a peak at around $M_V \sim -14$ and a sharp drop-off at $M_V > -10$, with essentially *no* satellites fainter than $M_V \sim -8$ predicted. This drop below $M_V > -8$ is not due to limited numerical resolution, but rather to the sharp assumed cooling cutoff at $T < 10^4$ K (because of our adopted atomic cooling function). However, at temperatures just slightly above the atomic cooling cutoff, cooling becomes quite rapid and so in the absence of some kind of feedback or suppression mechanism, these haloes rapidly cool all of the available baryons and convert them into stars.

In our models, photo-ionization due to a cosmic reionizing background and supernova feedback work together in order to re-shape this highly peaked luminosity function into the near-power law down to $M_V \sim -3$ that is implied by the recent SDSS observations. Photo-ionization suppresses the infall of hot gas into low-mass dark matter haloes, reducing the supply of baryons that are available for cooling and star formation, while SN feedback reheats cold gas and expels it from small haloes, again suppressing the efficiency of star formation. If we include only photo-ionization or only SN feedback, we find an excess of intermediate luminosity satellites and a shortage of ultra-faint satellites (see also Koposov et al. 2009). In agreement with previous works (e.g. Kravtsov et al. 2004), we find that the satellite luminosity function in our “standard” models depends only weakly on the assumed redshift of reionization.

We made use of results from the numerical hydrodynamic simulations of Gnedin (2000) to motivate our treatment of the suppression of gas infall due to the presence of a photo-ionizing background. A key parameter in this recipe is the “filtering mass”, or the halo mass below which the gas content is significantly reduced relative to the cosmic average. However, recent work by other groups (Okamoto et al. 2008; Hoesft et al. 2006) has found that the filtering mass may be considerably smaller than the results of Gnedin (2000) suggested. We investigate the implications of modifying the normalization and/or redshift dependence of the filtering mass as suggested by these works, and find that when a lower normalization of the filtering mass is adopted, the results are more sensitive to the redshift of reionization. We find that we can still reproduce the observed luminosity function with the lower filtering mass if we adopt a higher reionization redshift ($z_r \sim 11$ instead of $z_r \sim 7.5$).

We investigate the impact of stellar stripping on the observed luminosity function using the MORGANA model. We find that stellar stripping can only decrease the satellite stellar masses by at most about $\approx 20\%$, and therefore probably has only a minor effect on the satellite LF. However, we find that the modelling of tidal *destruction* of satellites does have a significant effect on faint end of the predicted LF.

In this work, we have concentrated on the comparison with observations of one particular quantity, the statistical distributions of satellite luminosity, although naturally the SAMs provide predictions of many other galaxy properties (e.g. Lagos et al. 2009). This has been done mainly for two reasons: first because robust state of the art obser-

vational data have recently been made available for those two quantities and second because our goal was to directly address the so called missing satellite problem and the origin of the newly discovered ultra-faint population. Other observed properties (such as metallicity, gas content, star formation history, etc.) contain complementary information on the formation mechanism of galactic satellites and more can be learned by studying them in details (e.g. Okamoto et al. 2009). While the objects produced in our SAMs do resemble several properties of observed satellites we have decided to defer a more extensive explorations of those properties to a future work.

The semi-analytic models that we use in this work were originally normalized to reproduce global quantities such as the field galaxy luminosity function or gas fractions for relatively luminous galaxies ($M_V \lesssim -16$). They have not previously been extensively tested against observations of galaxies on these very small mass scales. In the case of the K08 and S08 models, we found that the *identical* model ingredients and even parameter values used in the standard versions of these SAMs (e.g. Somerville et al. 2008, Kang et al. 2005) were also able to reproduce the MW satellite LF. In the case of the MORGANA model, we found that the SN feedback recipe in the original model (Monaco et al. 2007) had to be modified in order to reproduce the faint satellite population. In either case, we have gained important insights about the physical recipes incorporated in these models and their applicability over a wide range of galaxy mass scales.

Our study confirms and expands on previous works that address the so-called missing satellite problem using semi-analytic models and simulations. The main new contribution of our paper is the implementation of SAMs within merger trees extracted from numerical simulations with very high mass resolution (particle mass $m_p \sim 4 \times 10^5 h^{-1} M_\odot$), in which each of our four Galaxy-sized halo simulations contains 2–4 million particles. Thus, unlike previous studies (e.g. Benson et al. 2002; Somerville 2002; Kravtsov et al. 2004) which compared only with the “classical” satellite population $M_V = -9$, we can resolve the very small subhaloes that may host the newly detected population of ultra-faint satellites. We also have the advantage of multiple simulations, unlike studies based on the Via Lactea simulation (Diemand et al. 2007) alone. Although our results are in qualitative agreement with studies based on simpler analytic recipes for assigning baryons to dark matter (sub)-haloes (e.g. Koposov et al. 2009), we showed that in our models, the MW satellite LF is shaped by a complex combination of different physical processes including tidal destruction, photo-ionization, and supernova feedback.

Our models neglect several other physical processes that have been discussed in the literature, and which may be important in shaping the properties of galaxies on these mass scales. Although we model the suppression of gas infall by a uniform cosmic radiation field after reionization, we do not account for the modification of the atomic cooling function by the radiation field, the possible photo-evaporation of gas from small haloes after reionization (Barkana & Loeb 1999), or photo-ionization by the nearby large galaxy (i.e., the radiation field of the Milky Way; e.g. Weinmann et al. 2007). Perhaps most importantly, we neglect cooling via molecular hydrogen, and the associated complex and poorly understood possible positive and negative feedback effects con-

nected with the formation and destruction of H_2 (e.g. Salvadori & Ferrara 2009, Ricotti et al. 2008). The fact that our models are nevertheless able to reproduce the bulk of the ultra-faint satellite population *may* indicate that these other processes operate at second order or cancel each other out, or may be simply a fortuitous coincidence. Certainly this bears further study.

A further concern is that standard SAMs are known to fail to reproduce the more detailed properties of satellites in larger mass hosts: although they correctly reproduce the *number* of satellites as a function of halo mass, several different SAM codes (including the ones considered here) have been shown to produce too large a *fraction* of red and passive satellites (e.g. Kimm et al. 2008 and references therein) compared with observations. The main cause of this difficulty is believed to be the standard assumption that the hot gas halo is immediately stripped when a satellite enters a larger host, thereby depriving satellites of any new supply of gas (see Kang & van den Bosch 2008 for a detailed discussion and possible solution). It is unclear whether this will impact our predictions for the very low-mass MW satellites — we defer this question to a future investigation.

If we accept this “baryonic” solution of the “missing satellite problem”, other interesting implications follow. Our analysis predicts that roughly 1/5 of the total number of subhaloes with a present-day bound mass $M > 2 \times 10^7 M_\odot$ should be dark. In order to properly test this picture, a signature of the presence of these dark satellites is needed. One possibility is that they could be detected via gravitational lensing (e.g. Metcalf & Zhao 2002) since those small subhaloes will act as perturbers of the lensing signal coming from the main halo. Unfortunately recent results based on numerical simulations have shown that perturbations in the lensing potential induced by (dark) satellites are very small and unlikely to explain the anomalous flux ratios of some multiple lensed QSOs (Macciò et al. 2006; Macciò & Miranda 2006). Another possibility would be detection of γ -rays from dark matter annihilation, as the presence of substructure boosts the γ -ray signal by a factor of 4 to 15 relative to smooth galactic models (Diemand et al. 2008). Finally, a third possible opportunity to detect the presence of a significant dark population of subhaloes in the MW halo could come from the signatures of the interaction of such a population with the thin stellar streams in the MW halo (e.g. Odenkirchen et al. 2001, Ibata et al. 2002, Johnston et al. 2002, Grillmair & Dionatos 2006).

In final summary, our results show that not only is there no longer a “missing satellite problem”, but that well-known and well-motivated astrophysical processes working within the Λ CDM framework *naturally* predict the form of the observed MW satellite luminosity function over six orders of magnitude in luminosity. Indeed, it may be that convincing proof of the existence of the large predicted population of dark subhaloes via one of the methods suggested above (or one not yet discovered) is one of the last remaining major challenges for the Λ CDM paradigm.

ACKNOWLEDGEMENTS

The authors are grateful to Jelte de Jong, Anna Gallazzi, Nicholas Martin, Christian Maubetsch, Hans-Walter Rix

and Frank van den Bosch for many stimulating discussions. AVM thanks A. Knebe for his help with the AHF halofinder. Numerical simulations were performed on the PIA and on PanStarrs2 clusters of the Max-Planck-Institut für Astronomie at the Rechenzentrum in Garching and on the zBox2 supercomputer at the University of Zürich. Special thanks to B. Moore, D. Potter and J. Stadel for bringing zBox2 to life. FF and SK acknowledge the Kavli Institute for Theoretical Physics in Santa Barbara for hospitality: this research was partially supported by the National Science Foundation under Grant No. NSF PHY05-51164. SK was supported by the DFG through SFB 439 and by a EARA-EST Marie Curie Visiting fellowship.

REFERENCES

- Adelman-McCarthy, J. K., et al. 2008, *ApJS*, 175, 297
- Babul, A., & Rees, M. J. 1992, *MNRAS*, 255, 346
- Barkana, R., Loeb, A., 1999, *ApJ*, 523, 54
- Baugh, C. M. 2006, *Reports on Progress in Physics*, 69, 3101
- Belokurov, V., et al. 2007, *ApJ*, 654, 897
- Benson, A. J., Frenk, C. S., Lacey, C. G., Baugh, C. M., & Cole, S. 2002, *MNRAS*, 333, 177
- Bertschinger, E. 2001, *ApJS*, 137, 1
- Bullock J. S., Kravtsov A. V., Weinberg D. H., 2000, *ApJ*, 539, 517
- Chabrier G., 2003, *PASP*, 115, 763
- Diemand, J., Kuhlen, M., & Madau, P. 2007, *ApJ*, 667, 859
- Diemand, J., Kuhlen, M., Madau, P., Zemp, M., Moore, B., Potter, D., & Stadel, J. 2008, *Nature*, 454, 735
- Efstathiou, G. 1992, *MNRAS*, 256, 43P
- Fontanot, F., De Lucia, G., Monaco, P., Somerville, R. S., & Santini, P. 2009, *MNRAS*, 397, 1776
- Gilmore, G., Wilkinson, M. I., Wyse, R. F. G., Kleyna, J. T., Koch, A., Evans, N. W., & Grebel, E. K. 2007, *ApJ*, 663, 948
- Grillmair, C. J., & Dionatos, O. 2006, *ApJL*, 643, L17
- Hoeft, M., Yepes, G., Gottlöber, S., & Springel, V. 2006, *MNRAS*, 371, 401
- Ibata, R. A., Lewis, G. F., Irwin, M. J., & Quinn, T. 2002, *MNRAS*, 332, 915
- Irwin, M. J., et al. 2007, *ApJL*, 656, L13
- Johnston, K. V., Spergel, D. N., & Haydn, C. 2002, *ApJ*, 570, 656
- Kang, X., Jing, Y. P., Mo, H. J., Börner, G. 2005, *ApJ*, 631, 21
- Kang, X. 2008, *Proceedings of IAU 254 "The Galaxy Disk in Cosmological Context"*, arXiv:0806.3279
- Kang, X., & van den Bosch, F. C. 2008, *ApJL*, 676, L101
- Kimm, T., et al. 2009, *MNRAS*, 394, 1131
- Klypin, A., Kravtsov, A. V., Valenzuela, O., & Prada, F. 1999, *ApJ*, 522, 82
- Klypin, A., Zhao, H., & Somerville, R. S. 2002, *ApJ*, 573, 597
- Knollmann, S. R., & Knebe, A. 2009, *ApJS*, 182, 608
- Komatsu, E., et al. 2009, *ApJS*, 180, 330
- Koposov, S., et al. 2008, *ApJ*, 686, 279 (SK08)
- Koposov, S. E., Yoo, J., Rix, H.-W., Weinberg, D. H., Macciò, A. V., & Escudé, J. M. 2009, *ApJ*, 696, 2179
- Kravtsov, A. V., Gnedin, O. Y., & Klypin, A. A. 2004, *ApJ*, 609, 482
- Lagos, C. D. P., Padilla, N. D., & Cora, S. A. 2009, *MNRAS*, 397, L31
- Li, Y., Mo, H. J., van den Bosch, F. C., & Lin, W. P. 2007, *MNRAS*, 379, 689
- Li, Y.-S., Helmi, A., De Lucia, G., & Stoehr, F. 2009, *MNRAS*, 397, L87
- Lo Faro, B., Monaco, P., Vanzella, E., Fontanot, F., Silva, L., & Cristiani, S. 2009, *MNRAS*, 1225
- Macciò, A. V., Moore, B., Stadel, J., & Diemand, J. 2006, *MNRAS*, 366, 1529
- Macciò, A. V., & Miranda, M. 2006, *MNRAS*, 368, 599
- Macciò, A. V., Dutton, A. A., van den Bosch, F. C., Moore, B., Potter, D., & Stadel, J. 2007, *MNRAS*, 378, 55
- Macciò, A. V., Dutton, A. A., & van den Bosch, F. C. 2008, *MNRAS*, 391, 1940
- Macciò, A. V., Kang, X., & Moore, B. 2009, *ApJL*, 692, L109
- Madau, P., Kuhlen, M., Diemand, J., Moore, B., Zemp, M., Potter, D., & Stadel, J. 2008, *ApJL*, 689, L41
- Mainini, R., Macciò, A. V., Bonometto, S. A., & Klypin, A. 2003, *ApJ*, 599, 24
- Martin, N. F., Ibata, R. A., Chapman, S. C., Irwin, M., & Lewis, G. F. 2007, *MNRAS*, 380, 281
- Martin, N. F., de Jong, J. T. A., & Rix, H.-W. 2008, *ApJ*, 684, 1075 (MdJR08)
- Mateo, M. L. 1998, *ARA&A*, 36, 435
- McConnachie, A. W., et al. 2008, *ApJ*, 688, 1009
- Metcalf, R. B., & Zhao, H. 2002, *ApJL*, 567, L5
- Metz, M., Kroupa, P., & Jerjen, H. 2007, *MNRAS*, 374, 1125
- Monaco, P., Theuns, T., & Taffoni, G. 2002, *MNRAS*, 331, 587
- Monaco, P. 2004, *MNRAS*, 352, 181
- Monaco, P., Fontanot, F., & Taffoni, G. 2007, *MNRAS*, 375, 1189
- Moore, B., Ghigna, S., Governato, F., Lake, G., Quinn, T., Stadel, J., & Tozzi, P. 1999, *ApJL*, 524, L19
- Navarro, J. F., Frenk, C. S., & White, S. D. M. 1997, *ApJ*, 490, 493
- Odenkirchen, M., et al. 2001, *ApJL*, 548, L165
- Okamoto, T., Gao, L., & Theuns, T. 2008, *MNRAS*, 390, 920
- Okamoto, T., Frenk, C. S., Jenkins, A., & Theuns, T. 2009, arXiv:0909.0265
- Parkinson, H., Cole, S., & Helly, J. 2008, *MNRAS*, 383, 557
- Peñarrubia, J., McConnachie, A. W., & Navarro, J. F. 2008, *ApJ*, 672, 904
- Press, W. H., Teukolsky, S. A., Vetterling, W. T., & Flannery, B. P. 1992, *Cambridge: University Press*, —c1992, 2nd ed.,
- Quinn, T., Katz, N., & Efstathiou, G. 1996, *MNRAS*, 278, L49
- Read, J. I., Pontzen, A. P., & Viel, M. 2006, *MNRAS*, 371, 885
- Ricotti M., Gnedin N. Y., Shull J. M., 2002, *ApJ*, 575, 49
- Ricotti M., Gnedin N. Y., Shull J. M., 2008, *ApJ*, 685, 21
- Salvadori, S., & Ferrara, A. 2009, *MNRAS*, 395, L6
- Simon, J. D., & Geha, M. 2007, *ApJ*, 670, 313
- Somerville, R. S., Kolatt, T. S., *MNRAS*, 1999, 305, 1
- Somerville, R. S., Primack, J. R., *MNRAS*, 1999, 310, 1087

- Somerville, R. S., Primack, J. R., & Faber, S. M. 2001, MNRAS, 320, 504
- Somerville, R. S. 2002, ApJL, 572, L23
- Somerville, R. S., Hopkins, P. F., Cox, T. J., Robertson, B. E., & Hernquist, L. 2008, MNRAS, 391, 481
- Stadel, J. G. 2001, Ph.D. Thesis, University of Washington
- Strigari, L. E., Bullock, J. S., Kaplinghat, M., Diemand, J., Kuhlen, M., & Madau, P. 2007, ApJ, 669, 676
- Strigari, L. E., Bullock, J. S., Kaplinghat, M., Simon, J. D., Geha, M., Willman, B., & Walker, M. G. 2008, Nature, 454, 1096
- Taylor, J. E., & Babul, A., 2004, MNRAS, 348, 811
- Thoul, A. A., & Weinberg, D. H. 1996, ApJ, 465, 608
- Tollerud, E. J., Bullock, J. S., Strigari, L. E., & Willman, B. 2008, ApJ, 688, 277
- Walsh, S. M., Willman, B., & Jerjen, H. 2009, AJ, 137, 450
- Wechsler, R. H., Bullock, J. S., Primack, J. R., Kravtsov, A. V., & Dekel, A. 2002, ApJ, 568, 52
- Weinmann, S. M., Macciò, A. V., Iliev, I. T., Mellema, G., & Moore, B. 2007, MNRAS, 381, 367
- Willman, B., et al. 2005, ApJL, 626, L85
- Zentner, A. R., Bullock, J. S. 2003, ApJ, 598, 49
- Zentner, A. R., Berlind, A. A., Bullock, J. S., Kravtsov, A. V., Wechsler, R. H., 2005, ApJ, 624, 505
- Zucker, D. B., et al. 2006a, ApJL, 643, L103